# Assessment of Auto-Ignition Tendency of Gasoline, Methanol, Toluene and Hydrogen Fuel Blends in Spark Ignition Engines

Tim Franken, Lars Seidel, L. C. Mestre Gonzalez, Krishna Prasad Shrestha, A. Matrisciano, Fabian Mauss

# Assessment of Auto-Ignition Tendency of Gasoline, Methanol, Toluene and Hydrogen Fuel Blends in Spark Ignition Engines

T. Franken[1], L. Seidel[2], L. C. Mestre Gonzalez[1], K. P. Shrestha[1], A. Matrisciano[3] and F. Mauss[1]

[1]Brandenburg University of Technology Cottbus-Senftenberg, Cottbus, Germany.

E-mail: tim.franken@b-tu.de
Telephone: +(49) 160 97738595

[2]LOGE Deutschland GmbH, Cottbus, Germany.

E-mail: lars.seidel@logesoft.com

[3]Chalmers University of Technology, Goteborg, Sweden.

E-mail: andmatr@chalmers.se

**Abstract.** State of the art spark ignited gasoline engines achieve thermal efficiencies above 46 % e.g. due to friction optimized crank trains, high in-cylinder tumble flow and direct fuel injection. Further improvements of thermal efficiency are expected from lean combustion, higher compression ratio and new knock-resistant fuel blends. One of the limitations to these improvements are set by the auto-ignition in the end gas, which can develop to knocking combustion and severely damage the internal combustion engine. The auto-ignition is enhanced by high cylinder gas temperatures and reactive species in the end gas composition.

Quasi-dimensional Stochastic Reactor Model simulations with detailed chemistry allow to consider the thermochemistry properties of surrogates and complex end gas compositions. Based on the detailed reaction scheme and surrogate model, an innovative tabulated chemistry approach is utilized to generate dual-fuel laminar flame speed and combustion chemistry look-up tables. This reduces the simulation duration to seconds per cycle, while the loss in accuracy compared to solving the chemistry “online” is marginal. The auto-ignition events predicted by the tabulated chemistry simulation are evaluated using the Detonation Diagram developed by Bradley and co-workers. This advanced methodology for quasi-dimensional models evaluates the resonance between the shock wave and reaction-front velocity from auto-ignition in the end gas and determines if it is a harmful developing detonation or normal deflagration.

The aim of this work is to evaluate the auto-ignition characteristics of different fuel blends. The Stochastic Reactor Model with tabulated chemistry is applied to perform a numerical analysis of the auto-ignition of the fuel blends and operating conditions. Experimental measurements of a single cylinder research engine operated with RON95 E10 fuel are used to train and validate the simulation model. The RON95 E10 fuel is blended with Methanol, Hydrogen and Toluene. The knock tendency based on the evaluation of auto-ignition events of the different fuel blends are analysed for three operating points at 1500 *rpm* 15 *bar* IMEP, 2000 *rpm* 20 *bar* IMEP and 2500 *rpm* 15 *bar* IMEP with advanced spark timings.

## 1. Introduction

The research of alternative fuels for internal combustion engines covers aspects of fuel properties, production processes and availability of resources [1, 2]. One of the most straight forward approaches on producing alternative fuels with available resources, is the combination of excess wind or solar electric energy to produce Hydrogen ($H_2$) and Carbon Dioxide ($CO_2$) from the atmosphere or flue gases from industry processes [3, 4]. The captured $H_2$ can be directly burned in an internal combustion engine or further processed to produce Methane ($CH_4$) or Methanol ($CH_3OH$) [5, 6]. These fuels can

be directly burned in internal combustion engines, too, or further processed to long-chained hydrocarbon fuels.
The research group of Gschwend et al. [7] investigated the properties of 50 alternative fuels for spark ignition (SI) engine applications. They stated that tank-to-wheel $CO_2$ emissions are reduced for 2,2,3-Trimethylbutane, Butanol and Propanol isomers. While the lowest volumetric fuel consumption is found for 2-Phenylethanol and Anisole. However, some alternative fuels who show favourable properties for SI engine combustion, raise the threat of health for the environment. Yokoo et al. [8] investigated different fuel mixtures regarding their performance for lean combustion in SI engines. They stated that fuels like Anisole, Furan and Nitromethane are beneficial to extend the lean burn limit of two different internal combustion engines.
The focus of this work is set on Methanol, Toluene ($C_7H_8$) and Hydrogen mixed with a RON95 E10 surrogate as alternative fuels. The detailed chemistry of these fuels is well established and is applied to investigate the auto-ignition in the end gas. The analysis of the exhaust emissions is not considered since it would exceed the scope of this work. In the subsequent paragraphs selected properties of the fuels are reviewed that are beneficial for efficient SI engine operation. In **Table 1** some properties of the investigated fuels are summarized. The RON95 E10 surrogate is composed of iso-Octane, n-Heptane, Toluene and Ethanol (see **Table 3**). Ethanol and Methanol show the highest vaporization enthalpy ($h_{vap}$) at 300 *K* and smallest lower heating value (LHV). Toluene has the highest Research Octane Number (RON) and Motored Octane Number (MON), wherefore it is generally blended in gasoline fuels to reduce the knock tendency. Hydrogen shows the largest LHV value of the investigated fuels.

**Table 1**: Comparison of fluid properties [9, 10]. (*Determined at 300 K temperature.)

| **Fluid** | $\rho_{Norm}$ **[m³/kg]** | $h_{vap}$ **[kJ/kg] *** | **LHV [MJ/kg]** | **RON [-]** | **MON [-]** |
|---|---|---|---|---|---|
| Iso-Octane | 692 | 363 | 44.4 | 100 | 100 |
| n-Heptane | 684 | 364 | 44.6 | 0 | 0 |
| Ethanol | 789 | 919 | 26.7 | 111 | 94 |
| Methanol | 791 | 1166 | 19.9 | 109 | 89 |
| Toluene | 867 | 412 | 40.6 | 116 | 102 |
| Hydrogen | - | - | 120.1 | - | - |

In **Figure 1** the predicted laminar flame speeds of the investigated fuels using the detailed Ethanol Toluene Reference Fuel (ETRF) reaction scheme from the LOGEfuel package [11] are outlined. Detailed investigations of the reaction scheme performance can be found in the publications by Shrestha et al. [12, 13, 14, 15]. Hydrogen shows a significant higher laminar flame speed, which is why it is often considered in fuel blends to enhance the combustion. The laminar flame speed for Methanol is found to be slightly higher compared to RON95 E10 and Toluene. The research group of Ranzi et al. [16] published an extensive summary of laminar flame speeds for different alkanes, cyclo-alkanes, aromatics, alcohols and methyl ethers. They reported similar laminar flame speed ranges of Toluene and Methanol as it is shown in **Figure 1**. Veloo et al. [17] compared the laminar flame speed of Methane, Ethane, Ethanol and Methanol and reported that Methanol shows the highest flame speeds at stoichiometric and rich conditions. Mannaa et al. [18] performed an investigation of various Primary Reference Fuel (PRF), Toluene Reference Fuel (TRF), gasoline mixtures and neat species and its effect on the structure of the flame. They outlined that the laminar flame speed of Toluene is in the same range as iso-Octane, PRF and TRF mixtures at stoichiometric conditions. The increase of Hydrogen fraction in a Hydrogen – Carbon Monoxide – Air mixture is investigated by Dong et al. [19]. The increase of Hydrogen fraction increases the laminar flame speed for lean, stoichiometric, and rich mixture conditions.

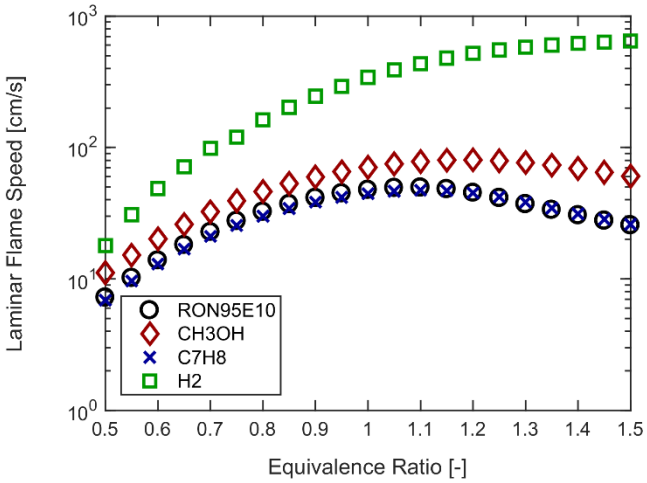


**Figure 1**: Comparison of predicted laminar flame speeds for different equivalence ratios for RON95 E10, Methanol, Toluene and Hydrogen at 30 bar and 600 K using an ETRF reaction scheme [11, 12, 13, 14, 15].

The predicted ignition delay times of RON95 E10, Methanol, Toluene and Hydrogen at 10 *bar* and $\phi$=1 are outlined in **Figure 2**. At low temperatures it is shown that the ignition delay times of Methanol, Toluene and Hydrogen are larger compared to RON95 E10. At high temperatures the ignition delay time of Toluene is similar to RON95 E10, while Methanol and Hydrogen show lower ignition delay times. Fieweger et al. [20] investigated the auto-ignition process of PRF mixtures, iso-Octane, n-Heptane and Methanol at elevated pressures and stoichiometric conditions. They showed that at high pressures of 40 *bar* and low temperatures the ignition delay time of Methanol is longer compared to iso-Octane, n-Heptane and PRF mixtures. At higher temperatures, the ignition delay times of Methanol are found in the same range as for n-Heptane. Burke et al. [21] performed an experimental campaign to measure the ignition delay times of different Methanol – Oxygen – Nitrogen – Argon mixtures. They stated that with an increasing fraction of Methanol in the mixture the ignition delay time is decreasing for temperatures between 833 *K* to 952 *K*. The influence of Toluene on the ignition delay time is outlined in the work from Andrae et al. [22]. They showed that the ignition delay times of Toluene are higher compared to TRF mixtures and n-Heptane at 30 *bar* and 50 *bar* pressures and stoichiometric conditions. Kéromnès et al. [23] measured the ignition delay time of Hydrogen and syngas mixtures at higher pressures. With increasing Hydrogen content in the syngas mixture, the ignition delay time is decreasing for different pressures and temperatures.

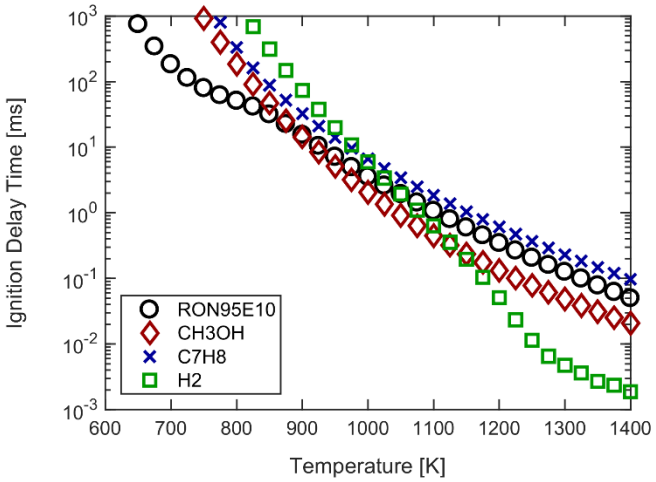


**Figure 2:** Comparison of predicted ignition delay times for different temperatures for RON95 E10, Methanol, Toluene and Hydrogen at 10 bar and $\phi$=1 using an ETRF reaction scheme [11, 12, 13, 14, 15].

The vapor-liquid saturation pressure and temperature of RON95 E10, Methanol and Toluene is compared in **Figure 3**. Toluene shows a similar vaporization characteristic as the RON95 E10 surrogate, while Methanol behaves significantly different. The normal boiling point of Methanol is at 337.6 *K*, while the boiling point of Toluene is at 383.7 *K*. The vaporization of Methanol has a significant effect on the auto-ignition characteristic in the end gas and shows an impact on the determination of the MON values as it is discussed by Spausta [24] and Seidel [25].

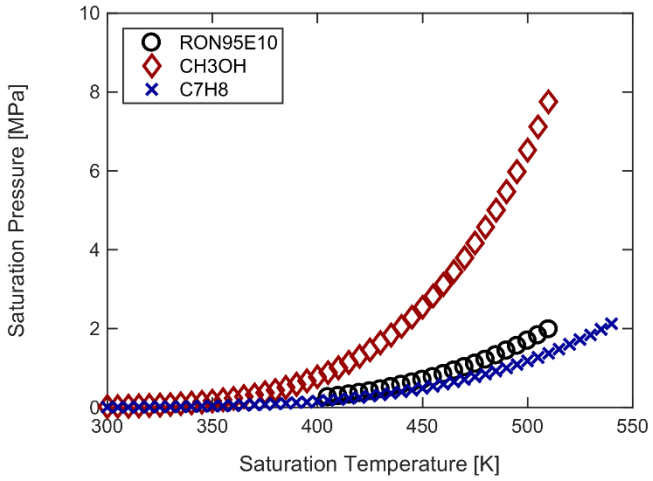


**Figure 3:** Comparison of the vapor-liquid saturation of RON95 E10, Methanol and Toluene [9].

In this work, the auto-ignition in the end gas for RON95 E10, Methanol, Toluene and Hydrogen mixtures is evaluated using the quasi-dimensional (QD) Stochastic Reactor Model (SRM) with tabulated chemistry and the Detonation Diagram developed by Bradley et al. [26, 27]. Netzer et al. [28, 29, 30, 31, 32] carried out extensive studies on the application of the Detonation Diagram with detailed chemistry to investigate the effect of different RON-MON sensitive fuels and operating conditions on the auto-ignition in SI engines. The Detonation Diagram method allows to evaluate different modes of auto-ignition that can occur in a SI engine and is established as a strong tool for knock analysis.
In the following section the fundamentals of the numerical method are introduced to provide an overview of the applied sub-models. Next, the experiments of the single cylinder research engine and QD-SRM model training are outlined. Finally, the simulation results are analysed and the effects of Methanol, Toluene and Hydrogen on the auto-ignition are discussed.

## 2. Methodology

### 2.1 Stochastic Reactor Model

The QD-SRM is based on a probability density function (pdf) approach for reactive flows [33, 34, 35]. The transport equation (1) of the pdf contains on the left side the accumulation term and various source terms $Q_i(\psi)$. These source terms include the piston work, convective heat transfer, chemical reactions, direct injection, and vaporization. Therein, $\boldsymbol{\Phi}$ is a vector of random variables, $\psi$ is its realization in the sample $\psi$-space and $t$ is the time. The term on the right-hand side $P_2$ describes the molecular mixing due to turbulence and is in a non-closed form.

$$\frac{\partial}{\partial \mathrm{t}} \mathrm{F}_{\boldsymbol{\Phi}}(\psi, \mathrm{t}) + \frac{\partial}{\partial \psi_\mathrm{i}} \left( \mathrm{Q}_\mathrm{i}(\psi) \mathrm{F}_{\boldsymbol{\Phi}}(\psi, \mathrm{t}) \right) = \mathrm{P}_2 \mathrm{F}_{\boldsymbol{\Phi}}(\psi, \mathrm{t}) \tag{1}$$

The Curl mixing model [36] is incorporated to close the term $P_2$ in equation (2). The mixing model contains the turbulent mixing time $\tau$, to account for turbulence-chemistry interaction [37, 38], the training parameter $C_{\boldsymbol{\Phi}}$ and the decay parameter $\beta$, which is set to 1.

$$\mathrm{P_2F_{\Phi}}(\psi,\mathrm{t}) = \frac{\mathrm{C_{\Phi}}\beta}{\tau} \cdot \left[ \int_{\Delta\psi} F_{\Phi}(\psi - \Delta\psi, t) F_{\Phi}(\psi + \Delta\psi) d(\Delta\psi) - F_{\Phi}(\psi, t) \right] \tag{2}$$

The turbulent mixing time is calculated using the QD K-k turbulence model developed by Dulbecco et al. [39]. The model solves equations for kinetic energy in equation (3) and turbulent kinetic energy in equation (4).

$$\frac{\mathrm{dK}}{\mathrm{dt}} = 0.5 \cdot C_{tke} \cdot \frac{\dot{m}_{in}}{m_{total}} \cdot v_{in}^2 + C_{inj} \cdot \frac{dK_{inj}}{dt} + K \cdot \frac{\dot{m}_{out}}{m_{total}} + C_{comp} \cdot K \cdot \frac{\dot{\rho}}{\rho} - P_k - K \cdot \left( \frac{\dot{\rho}}{\rho} + \frac{\dot{V}}{V} \right) \tag{3}$$

$$\frac{\mathrm{dk}}{\mathrm{dt}} = 0.5 \cdot (1 - C_{tke}) \cdot \frac{\dot{m}_{in}}{m_{total}} \cdot v_{in}^2 + C_{inj} \cdot \frac{dk_{inj}}{dt} + k \cdot \frac{\dot{m}_{out}}{m_{total}} + C_{comp} \cdot k \cdot \frac{\dot{\rho}}{\rho} + P_k - k \cdot \left( \frac{\dot{\rho}}{\rho} + \frac{\dot{V}}{V} \right) - C_{diss} \cdot \varepsilon \tag{4}$$

In these equations, $\dot{m}_{in}$ is the intake valve mass flow, $m_{total}$ is the trapped cylinder mass, $t$ is the time in seconds, $v_{in}$ is the intake valve flow velocity, $K_{inj}$ is the kinetic energy from the direct injection, $\dot{m}_{out}$ is the exhaust valve mass flow, $\dot{\rho}$ is the change of density, $\rho$ is the density, $\dot{V}$ is the change of cylinder volume and $V$ is the instantaneous cylinder volume. The dissipation $\varepsilon$ in equation (5) is derived from the turbulent kinetic energy and integral length scale $l_I$, which is based on the instantaneous cylinder volume and calculated in equation (6).

$$\varepsilon = \frac{2}{3} \cdot \frac{\mathrm{k}^{\frac{3}{2}}}{\mathrm{l_I}} \tag{5}$$

$$\mathrm{l_I} = C_{len} \cdot V^{\frac{1}{3}} \tag{6}$$

The term $P_k$ is a production term for turbulent kinetic energy from tumble motion decay. The equation is outlined in (7).

$$\mathrm{P_k} = 0.3307 \cdot C_{\beta} \cdot l_I \cdot k^{\frac{1}{2}} \cdot \frac{K}{\Delta^2} \tag{7}$$

Therein, $\Delta$ is a measure for the size of the tumble vortex and is calculated by $\Delta = min(C_{\Delta,1} \cdot V^{\frac{1}{3}}, C_{\Delta,2} \cdot min(h_{cyl}, d_{bore}))$, with the piston-head distance $h_{cyl}$ and the cylinder bore $d_{bore}$. The turbulent mixing time is finally calculated using equation (8).

$$\tau = \frac{\mathrm{k}}{\varepsilon} \tag{8}$$

The parameters $C_{inj}$, $C_{comp}$, $C_{tke}$, $C_{diss}$, $C_{len}$, $C_{\beta}$, $C_{\Delta,1}$, $C_{\Delta,2}$ and $C_{\Phi}$ are model constants and need to be trained for the respective engine.
To solve the pdf transport equation the gas within the cylinder is discretized in notional particles, each containing its own composition and temperature (see **Figure 4**).

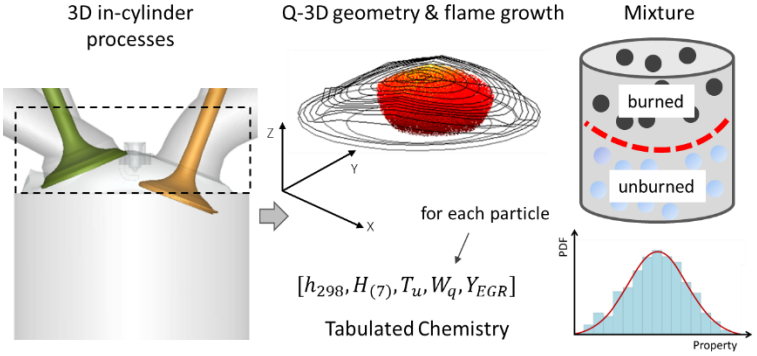


**Figure 4:** Concept of the two-zone SRM for spark-ignition engines [37].

The QD-SRM uses a two-zone approach and the auto-ignition in the end gas and chemistry in the burned zone for emission formation are retrieved from the pre-compiled look-up tables. The flame front propagates based on turbulent flame speed $s_T$, which is calculated retrieving the laminar flame speed $s_L$ from the pre-compiled look-up tables. The turbulent flame speed is calculated with equation (9) based on the model by Peters et al. [40].

$$\frac{s_T}{s_L} = 1 + C \cdot \left(\frac{u'}{s_L}\right)^m \tag{9}$$

Therein, $C$ and $m$ are model constants. $u'$ is the turbulence intensity and is calculated based on the scalar mixing time. Additionally, the flame front is traced based on a polygonal approach to account for flame-wall-interactions (see Q-3D geometry & flame growth in **Figure 4**) [41]. The values of the model constants are outlined in **Table 2**. Those constants were tested in previous works for different gasoline engines and are not changed during the present work. The QD-SRM accounts for cycle-to-cycle variations in the cylinder gas composition and temperature induced by stochastic mixing and stochastic heat transfer processes [42]. The Woschni heat transfer correlation in equation (10) with base parameters and wall temperatures of 450 *K* is used to calculate the heat transfer coefficient $\alpha$ [43].

$$\alpha = C_{pre} \cdot d^{-0.2} \cdot p^{0.8} \cdot T^{-0.53} \cdot \left[C_1 \cdot c_m + C_2 \frac{V \cdot T_0}{p_0 \cdot V_0} \cdot (p - p_{mot})\right] \tag{10}$$

Therein, $C_{pre}$, $C_1$ and $C_2$ are model constants, $d$ is the engine bore, $p$ is the cylinder pressure, $T$ is the cylinder temperature, $c_m$ is the mean piston speed, $p_{mot}$ is the motored cylinder pressure and $V$ is the cylinder volume. The index $0$ highlights parameters at reference conditions. The heat transfer model constants are tested in previous works for different gasoline engines and are not changed during the present work. The QD-SRM model setup is shown in **Table 2**.

**Table 2**: QD-SRM model setup.

| **Parameter** | **Value** |
|---|---|
| Number of Particles | 500 |
| Time Step Size | 0.5 °*CA* |
| Number of Cycles | 30 |
| $C_{pre}$ | 1.0 |
| $C_1$ | 2.28 |
| $C_2$ | 0.0065 |
| $C$ | 2.5 |
| $m$ | 0.9 |

### 2.2 Tabulated Chemistry

The tabulated chemistry is based on the detailed ETRF reaction scheme from the LOGEfuel package [11] consisting of 690 species and 8278 reactions. The detailed reaction scheme is validated for different experiments and for engine relevant conditions [12, 13, 14, 15], which is highlighted for one set of experiments from Jerzembeck et al. [44] in **Figure 5** using the RON95 E10 surrogate from **Table 4**.

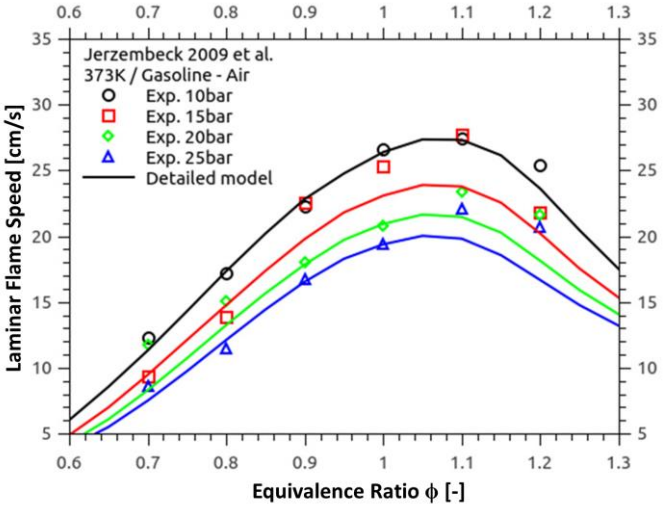


**Figure 5:** Comparison of predicted laminar flame speeds using the detailed reaction scheme from the LOGEfuel package [11] and experiments with gasoline as fuel from Jerzembeck et al. [44] at 373 K and different pressures, with air as oxidizer. Measurement accuracy is within ±4 cm/s. The symbols highlight the experiments and the lines show the simulations.

A dual fuel approach for the surrogate and second fuel is used. The composition of the first fuel stream is outlined in **Table 3** in liquid volume fraction. The second fuel stream is composed of Methanol, Toluene or Hydrogen.

**Table 3:** Surrogate composition in liquid volume fraction for the reference ETRF fuel.

| Fuel | Iso-Octane | n-Heptane | Ethanol | Toluene |
|---|---|---|---|---|
| RON95 E10 | 0.44 | 0.141 | 0.101 | 0.318 |

The comparison of the properties of the experimental RON95 E10 fuel and the surrogate are outlined in **Table 4**. The QD-SRM is trained and validated for single cylinder engine experiments using the RON95 E10 fuel.

**Table 4:** Comparison of the properties of the experimental RON95 E10 fuel and the surrogate.

| | Experiment | Surrogate |
|---|---|---|
| **RON** | 96.7 | 96.7 |
| **MON** | 85.8 | 87.4 |
| **C:H:O** | 6.6:12.8:0.21 | 6.3:11.8:0.21 |
| **Density** | 748.7 *kg/m³* | 756.4 *kg/m³* |
| **LHV** | 41.78 *MJ/kg* | 41.14 *MJ/kg* |

The laminar flame speeds and the combustion chemistry are stored in a pre-compiled look-up table (see table ranges in **Table 5** and **Table 6**) using the software LOGEtable [10]. The table ranges are optimized to reduce the size of the tables but to keep a high resolution of auto-ignition sensitive conditions, e.g. the Negative Temperature Coefficient (NTC) region. During the simulation, laminar flame speeds and chemistry sources are retrieved from the look-up tables based on the current thermodynamic conditions.
Furthermore, a progress variable approach is used for the chemistry table look-up [45, 46, 47, 48]. The progress variable $C$ is defined as follows in equation (11).

$$\mathrm{C} = \frac{\mathrm{h}_{298} - \mathrm{h}_{298,\mathrm{u}}}{\mathrm{h}_{298,\mathrm{max}} - \mathrm{h}_{298,\mathrm{u}}} \tag{11}$$

Therein, $h_{298}$ is the latent enthalpy calculated at 298 *K*, and summed over all species, subscript $u$ denotes unburned state, and subscript $max$ denotes the most reacted state, which is assumed to be where the maximum chemical heat is released.

**Table 5:** Laminar flame speed dual fuel table specifications.

| Parameter | Range | Steps |
|---|---|---|
| Temperature | 350 – 1400 *K* | 50 *K* |
| Pressure | 1 – 150 *bar* | 1 .. 10 *bar* |
| Equivalence Ratio | 0.5 – 1.5 | 0.05 |
| Fuel Fraction | 50 – 100 *%* | 10 *%* |
| EGR | 0 – 40 *%* | 10 *%* |

**Table 6:** Combustion chemistry dual fuel table specifications.

| Parameter | Range | Steps |
|---|---|---|
| Temperature | 250 – 1400 *K* | 10 .. 50 *K* |
| Pressure | 1 – 200 *bar* | 5 .. 20 *bar* |
| Equivalence Ratio | 0.2 – 4.0 | 0.2 .. 0.25 |
| Fuel Fraction | 50 – 100 *%* | 10 *%* |
| EGR | 0 – 10 *%* | 10 *%* |

### 2.3 Resonance Theory

The resonance theory for the QD-SRM is introduced by Netzer [28]. Based on syngas (mixtures of $H_2$/CO) experiments and One-Dimensional (1D) CFD simulations, Bradley et al. [26] developed the Detonation Diagram in **Figure 6**.

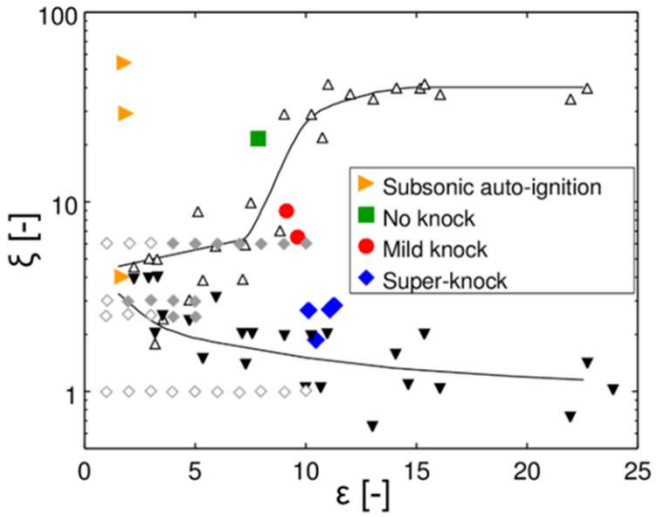


**Figure 6:** Detonation Diagram; Full (▼) and hollow triangles (Δ) and lines: experiments and simulations by Bradley et al. [26]; Full (♦) and hollow (◊) diamonds one-dimensional simulations by Peters et al. [49]: hollow symbols: no detonation, filled symbols: developing detonation; Full symbols (►, ■, ●, ♦) LES engine simulations by Bates et al. [50].

The Detonation Diagram evaluates the characteristics of the auto-ignition in the end gas with two dimensionless parameters. $\xi$ is the ratio of the speed of sound $a$ and the apparent reaction-front velocity $u$ [27] in equation (12). The apparent reaction-front velocity can be calculated using the temperature gradient over the travel distance $x$ and the gradient of the ignition delay time $\tau$.

$$\xi = \frac{\mathrm{a}}{u} = a\frac{\delta T}{\delta x}\frac{\delta \tau}{\delta T} \tag{12}$$

With the help of the resonance parameter $\xi$, the characteristic of the auto-ignition event can be separated into different modes. If $u < s_L$, a normal flame occurs driven by heat conduction and diffusion, which is called deflagration [51, 52]. If $s_L < u < a$, a subsonic auto-ignition occurs, which is harmless for the engine. If $u > a$, thermal explosion is observed, which usually does not occur under conven-

tional SI engine operating conditions. To form a developing detonation, $u$ and $a$ must be of the same order of magnitude ($u \approx a$). The order of magnitude increases with higher reactivity of the mixture and is calculated with the reactivity parameter $\varepsilon$ in equation (13).

$$\varepsilon = \frac{\mathrm{l}}{a \cdot \tau_e} \tag{13}$$

Here, $l$ is the length of the constant temperature gradient kernel before the auto-ignition occurs and $\tau_e$ is the excitation time, which is the time between 5 % to maximum heat release of the auto-ignition event. The denominator describes how far the sound wave travels during the ignition event. Evaluated with the length of the constant temperature gradient, $\varepsilon$ is a non-dimensional length, which can be interpreted as the dimensionless ignition kernel size. With higher $\varepsilon$ and increasing kernel size accordingly, the range of conditions that lead to a developing detonation are getting wider. The limits of the different modes of reaction-front propagation in **Figure 6** are experimentally and numerically obtained for syngas [26]. To make it applicable for engine conditions, Peters et al. [49] evaluated the regime limits for n-heptane and iso-octane. Since, these modes are chemically dependent on the high temperature chemistry, they appear in the same range for all reviewed fuels. Bates et al. [50] applied this evaluation method to 3D Large Eddy Simulation (LES) and characterized typical areas in the Detonation Diagram that cover engine operating conditions from harmless subsonic auto-ignition over non-knock and mild-knock to super-knock.
Kalghatgi and Bradley [53] investigated pre-ignition and super-knock events for a turbo-charged SI engine. To evaluate the severity of an auto-ignition event based on the Detonation Diagram they proposed the equation (14), which relates the dimensionless expression of the overpressure to the resonance parameter.

$$\frac{\mathrm{p(t)}_{max}}{p} \sim \left(\frac{1}{\xi}\right)^2 \tag{14}$$

Subsequently, they calculated $\xi = 8.8$ and $\varepsilon = 9.1$ for an auto-ignition, which is classified as heavy knock. Those values are used in this work for the definition of the knock limit.

## 3. Experiments

The experiments are conducted on a single cylinder research engine at the TU Berlin. The single cylinder engine is built up for fundamental investigations of port and direct water injection in the FVV project "Water Injection in SI engines" [7, 13, 46, 50]. The engine specifications are depicted in **Table 7**.

**Table 7:** Technical specifications of single cylinder research engine.

| **Parameter** | **Value** |
|---|---|
| Bore | 71.9 mm |
| Stroke | 82 mm |
| Compression Ratio | 10.75 : 1 |
| Number of Valves | 4 |
| Fuel Injection | Central Direct |

The engine experiments are conducted using a central direct fuel injection. The position of the injector is shown in **Figure 7**. More details on the experimental campaign can also be found in the work of Kauf et al. [50].

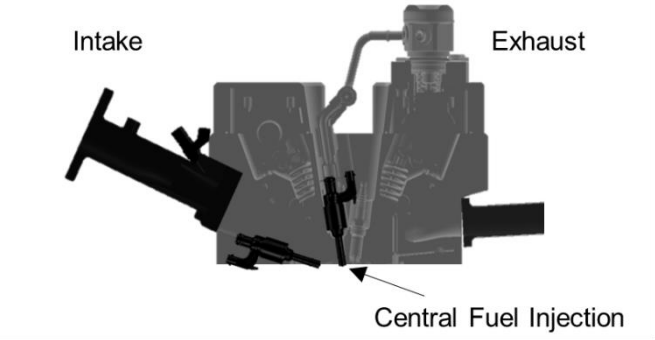


**Figure 7:** Position of the central fuel injection of the single cylinder research engine at TU Berlin [50].

The engine is equipped with low-pressure and high pressure sensors to measure the cylinder and manifold pressures of 250 consecutive cycles. The simplified testbench scheme and positions of the pressure ($p$), temperature ($T$), air-fuel ratio ($\lambda$), mass flow ($\dot{m}$) sensors and emission analyzers are shown in **Figure 8**. The intake system consists of a compressor unit to set the boost pressure, a Sensyflow for air mass flow measurement, a throttle, a mixing tank and two intake runners. The exhaust system consists of two exhaust runners, an exhaust orifice to control the back pressure, a diffusor, and an exhaust ventilation.

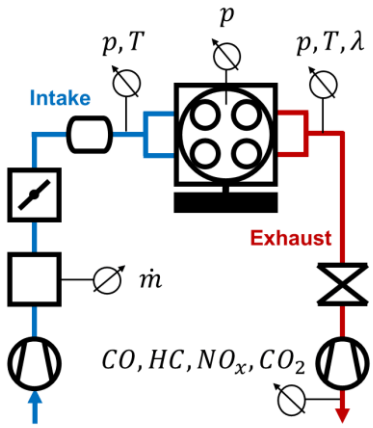


**Figure 8:** Single cylinder research engine testbench scheme from TU Berlin [46].

## 4. Model Training

The 1D-QD-SRM model training strategy is outlined in **Figure 9**. First, the air path system parameters of the 1D model are trained to fit the simulated intake system pressure frequency ($f_{p,intake}$) and amplitude ($A_{p,intake}$) and exhaust system pressure frequency ($f_{p,exhaust}$) and amplitude ($A_{p,exhaust}$). This is done by adjusting the discharge coefficients of the throttle ($C_{D,throttle}$), the intake and exhaust ports ($C_{D,port}$) and the exhaust orifice ($C_{D,orifice}$). Second, the fired operating points are used to fit the closed cycle in-cylinder pressure of the experiments. A multi-objective genetic optimization process is applied using modeFRONTIER [54]. The objectives of the optimization are to minimize the sum of least squares of cylinder pressure ($\varepsilon_{P\ ressure}$), maximum cylinder pressure ($\varepsilon_{PCP}$), crank angle of maximum cylinder pressure ($\varepsilon_{PCPCA}$) and CO emissions at exhaust valve opening (EVO) ($\varepsilon_{CO,EVO}$). The QD-SRM turbulence model parameters $C_\Phi$ and $C_{inj}$ are the optimization input parameters. Subsequently, the QD-SRM model parameters are validated using the remaining fired operating points. More information about the model training and validation results can be found in the work published by Franken et al. [55].

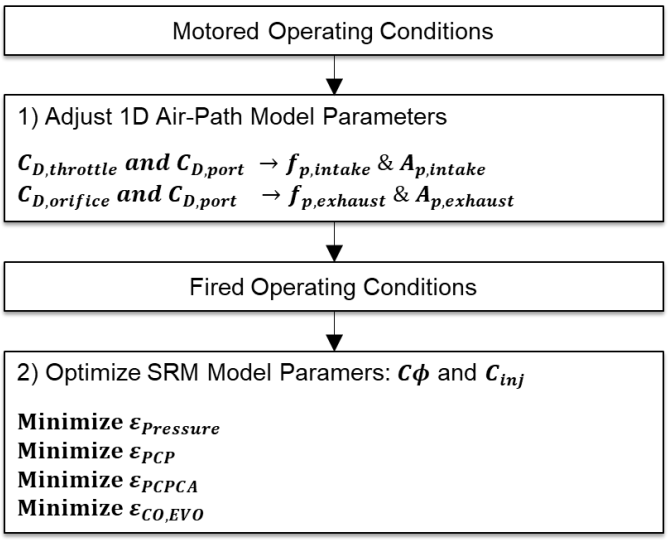


**Figure 9:** QD-SRM model training procedure.

The final model parameters of the QD-SRM turbulence model in equation (3) and (4) are shown in **Table 8**. Mostly the same turbulence model parameters are used, as reported by Dulbecco et al. [35].

**Table 8:** QD-SRM turbulence model parameters.

| Parameter | Value |
|---|---|
| $C_{inj}$ | 0.005 |
| $C_{comp}$ | 0.67 |
| $C_{tke}$ | 0.85 |
| $C_{diss}$ | 1.0 |
| $C_{len}$ | 0.3 |
| $C_{\beta}$ | 0.25 |
| $C_{\Delta,1}$ | 0.073 |
| $C_{\Delta,2}$ | 0.1313 |
| $C_{\Phi}$ | 4.65 |

## 5. Results and Discussion

In this work the effect of Methanol, Toluene and Hydrogen addition to the RON95 E10 surrogate in a SI engine is investigated with the focus on auto-ignition in the end gas. While the effect of vaporization enthalpy is considered of those fuels, the air, RON95 E10 and fuel mixture is assumed to be homogeneously mixed to simplify the problem. In the future the effect of inhomogeneous mixtures on the auto-ignition in a SI engine will be investigated. Further, it is assumed that the different fuel blends do not affect the flame-turbulence interaction and one set of model parameters is used for all fuel blends to calculate the turbulent flame speed in equation (9).
First, the QD-SRM model training results are outlined for the measured motored and fired operating points in **Table 9**.

**Table 9:** QD-SRM engine operating points used for auto-ignition analysis.

| OP | Speed | IMEP | $\lambda$ | ST |
|---|---|---|---|---|
| 1 | 1500 *rpm* | 15 *bar* | 1.0 | -4.4 °*CA* |
| 2 | 2000 *rpm* | 20 *bar* | 1.0 | 1.5 °*CA* |
| 3 | 2500 *rpm* | 15 *bar* | 1.0 | -9.7 °*CA* |

Second, the spark timing of the three operating points is adjusted to achieve center of combustion at 8 °*CA*, which is defined as Maximum Break Torque (MBT). To keep the IMEP and air-to-fuel ratio ($\lambda$) constant during the parameter variations, the charge pressure is modified (see **Figure 10**). Third, the fuels Methanol ($CH_3OH$), Toluene ($C_7H_8$) and Hydrogen ($H_2$) are added to the surrogate and the auto-ignition is evaluated using the Detonation Diagram. Hereby, Methanol and Toluene are added to the fuel blend to suppress auto-ignition, while Hydrogen is added to advance center of combustion.

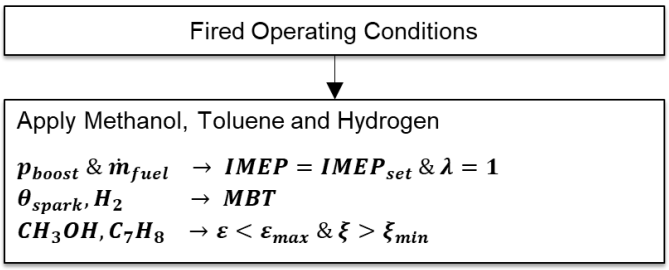


**Figure 10:** QD-SRM strategy to adjust the operating point to MBT at the knock limit.

The amount of Methanol, Toluene and Hydrogen addition is quantified based on mass using the fuel fraction (FF) definition in equation (15). Therein, $m_i$ describes the absolute mass of the additional fuel (Methanol, Toluene or Hydrogen) and $m_{RON95E10}$ describes the absolute mass of the base fuel (RON95 E10). The sum of the two masses equals to the total mass of fuel in the cylinder.

$$FF_i = \frac{m_i}{m_{RON95E10}} \cdot 100\% \tag{15}$$

### 5.1 Training Results

In **Figure 11** the in-cylinder pressure and heat release rate of the experiments are compared to the QD-SRM training results. The simulation closely matches the pressure during the high pressure phase and valve opening time. Some deviations are found for the operating point at 2000 *rpm* and 20 *bar* IMEP, where the simulation predicts an earlier start of combustion. The exhaust emissions are not the focus of this work, but a comparison with the measured exhaust emissions of the trained model can be found in the publication by Franken et al. [55] and [56].

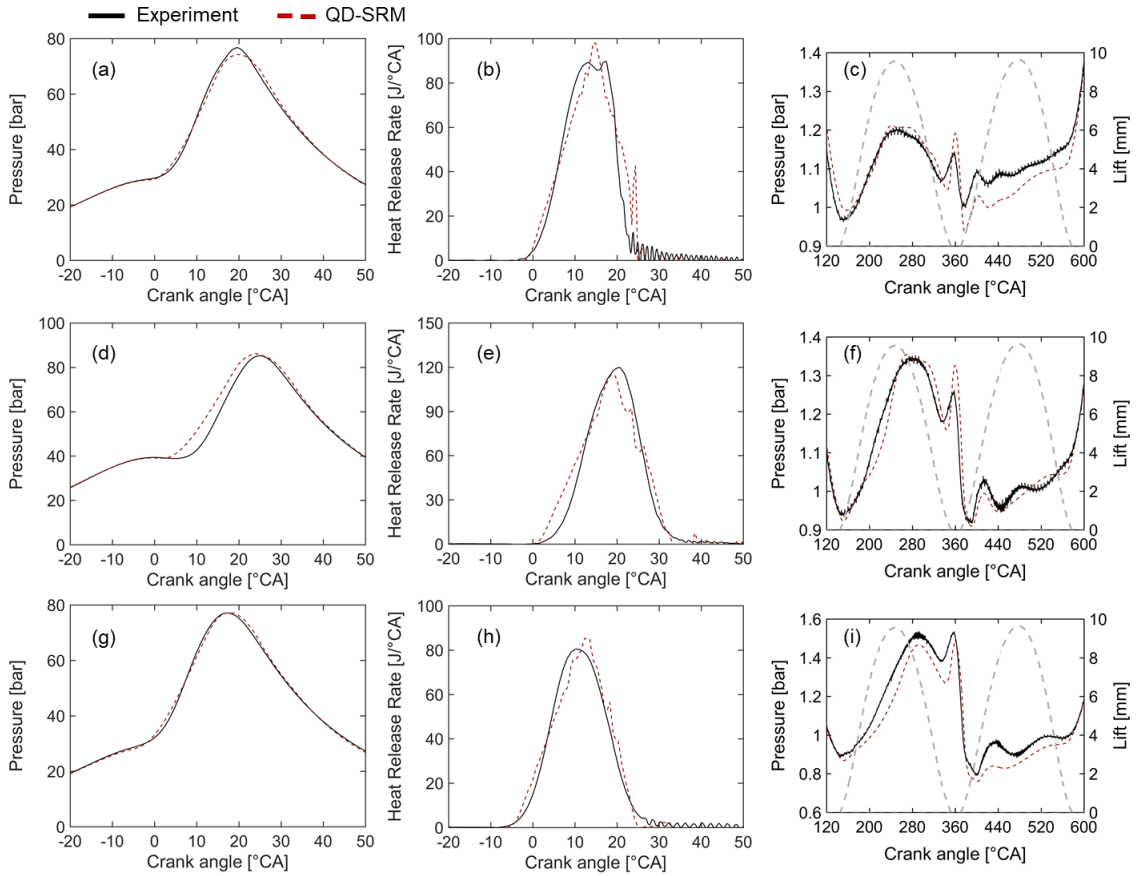


**Figure 11:** QD-SRM simulation results of in-cylinder pressure, heat release rate and pressure during valve opening compared to the experiments for three fired operating points: (a) – (c) 1500 rpm 15 bar IMEP, (d) – (f) 2000 rpm 20 bar IMEP and (g) – (i) 2500 rpm 15 bar IMEP. Fired TDC is at 0 °CA.

### 5.2 Spark Timing Sweep

In **Figure 12** the simulation results of a spark timing sweep for all three operating points are outlined. With the advanced spark timing the peak cylinder pressure (PCP) is increased up to 100 *bar* to 130 *bar* and the center of combustion is shifted towards MBT (8 °*CA*). The heat release rate (Norm. u-RoHR) in **Figure 12 (b), (e) and (f)** is normalized by the mass of the air-fuel mixture in the end gas to exclude the effect of changing end gas mass. The maximum heat release rates of 9x10$^5$ *J/kg/°CA* to 10x10$^5$ *J/kg/°CA* are found for 1500 *rpm* 15 *bar* IMEP and 2000 *rpm* 20 *bar* IMEP since these operating points are found by experiments and simulations to be at the knock limit. Further, the strong increase of the heat release rate cause a strong rise in the temperature in the end gas from 1000 *K* to 2500 *K*.

The Detonation Diagram in **Figure 13 (a) to (c)** shows the change of the auto-ignition strength for different spark timings and operating points. The resonance parameter and reactivity parameter are averaged for 30 stochastic cycles of the QD-SRM simulation to obtain a statistical stable result. The auto-ignition at the latest spark timing is found to be in deflagration mode for all operating points, where the reaction front of the auto-ignition propagates at laminar flame speed [51]. With advanced spark timing the combustion of the air-fuel mixture is promoted and auto-ignition in the end gas occurs at higher local temperatures. As a result, the mixture becomes more reactive and the reaction front propagates at subsonic conditions. For the operating points at 1500 *rpm* 15 *bar* IMEP and 2000 *rpm* 20 *bar* IMEP it is predicted that the auto-ignition develops to a detonation (knocking combustion) with a spark timing shift between 4 °*CA* to 6 °*CA* compared to the base spark timing. For 2500 *rpm* 15 *bar* IMEP the spark timing shift is found between 6 °*CA* and 8 °*CA* since this operating point is not at the knock limit.

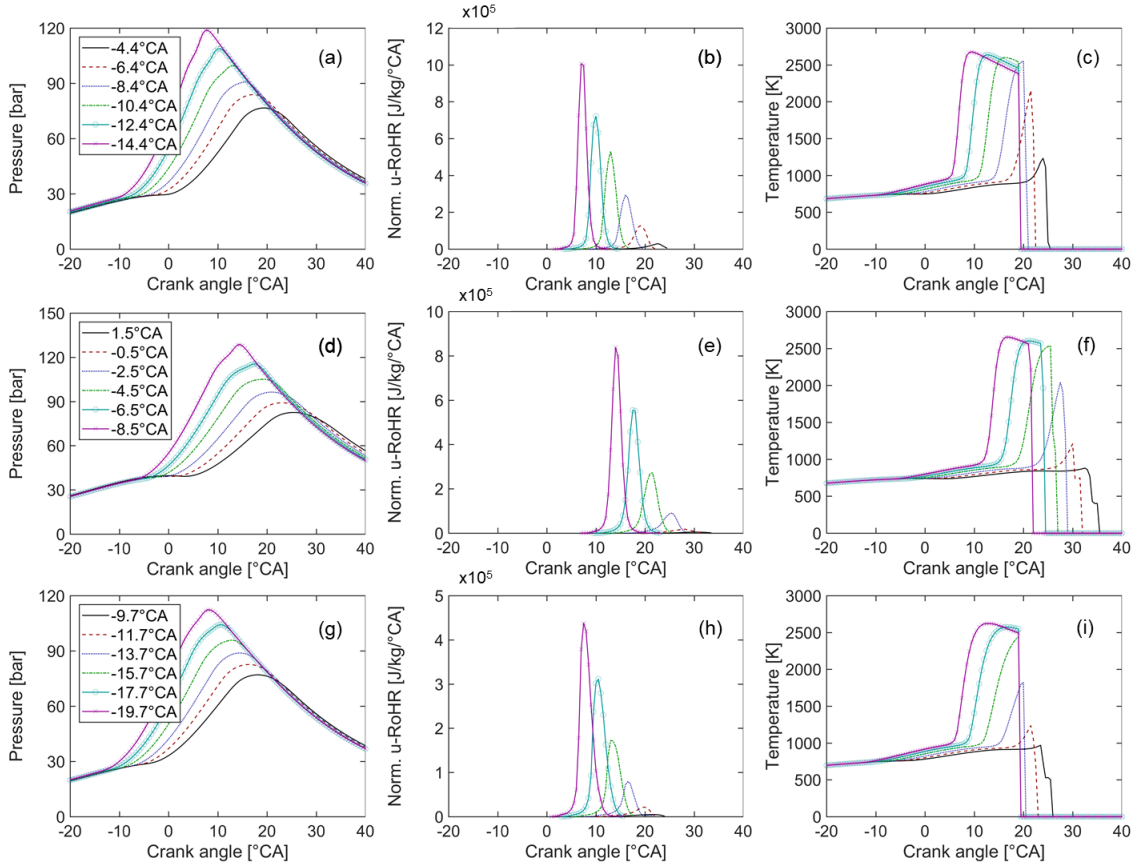


**Figure 12:** QD-SRM simulation results of in-cylinder pressure, normalized heat release rate in the end gas and temperature in the end gas for a spark timing sweep: (a) – (c) 1500 rpm 15 bar IMEP, (d) – (f) 2000 rpm 20 bar IMEP and (g) – (i) 2500 rpm 15 bar IMEP. Fired TDC is at 0 °CA.

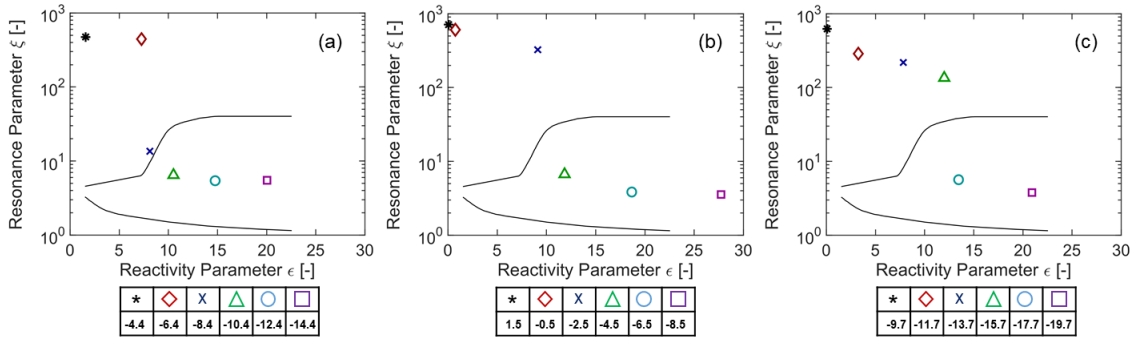


**Figure 13:** QD-SRM simulation results of the detonation diagram for a spark timing sweep: (a) 1500 rpm 15 bar IMEP, (b) 2000 rpm 20 bar IMEP and (c) 2500 rpm 15 bar IMEP.

The MBT spark timing is determined for all three operating points. For 1500 *rpm* 15 *bar* IMEP a spark timing of -9.4 °*CA* is found, for 2000 *rpm* 20 *bar* IMEP a spark timing of -8.5 °*CA* is found and for 2500 *rpm* 15 *bar* IMEP a spark timing of -14.7 °*CA* is found. The addition of Methanol and Toluene is investigated in the subsequent sections to reduce the strength of auto-ignition at MBT. Further, the addition of Hydrogen is investigated to promote combustion and achieve MBT operating conditions.

### 5.3 Effect of Methanol Addition

In **Figure 14** the simulation results of different Methanol fuel fractions for different operating conditions are shown. The increasing amount of Methanol fraction in the fuel blend shows a decreasing trend for the normalized heat release rate and temperature in the end gas. On the one hand side, this

is caused by the higher vaporization enthalpy of Methanol compared to RON95 E10 (see **Table 1**), and on the other hand side by the changed reactivity of the end gas mixture. The decreased auto-ignition heat release rate is in good agreement with the higher RON value of Methanol (see **Table 1**).
The detonation diagram in **Figure 15 (a) to (c)** supports this trend because the auto-ignition is moved from the developing detonation to subsonic auto-ignition and deflagration mode. For 1500 *rpm* 15 *bar* IMEP it is found that the addition of 10 *%* to 30 *%* Methanol fuel fraction to the fuel blend is required to obtain non-knocking combustion. For 2000 *rpm* 20 *bar* IMEP the Methanol fuel fraction in the fuel blend is determined with 50 *%* to 80 *%*.
The effect of the vaporization enthalpy of Methanol on auto-ignition is outlined in **Figure 15 (d) to (f)**. For the simulation results shown, the vaporization enthalpy of Methanol is neglected and only the effect of changed reactivity due to different end gas mixtures is accounted for. The addition of 10 *%* to 50*%* Methanol fuel fraction to the mixture showed an increasing reactivity for 1500 *rpm* 15 *bar* IMEP operating conditions. For 2500 *rpm* 15 *bar* IMEP the 10 *%* to 100 *%* Methanol fuel fraction addition increased the reactivity and reaction front velocity. Overall, the vaporization enthalpy of Methanol is found to have a strong effect on the shift of auto-ignition from a developing detonation to deflagration since it reduces the local temperature at which auto-ignition occurs. Those effects are also supported by earlier works (e.g. Spausta [24] and Seidel [25] and works cited therein) who outlined the large deviation of RON and MON values for Methanol and Ethanol due to vaporization at elevated temperatures in the MON test.

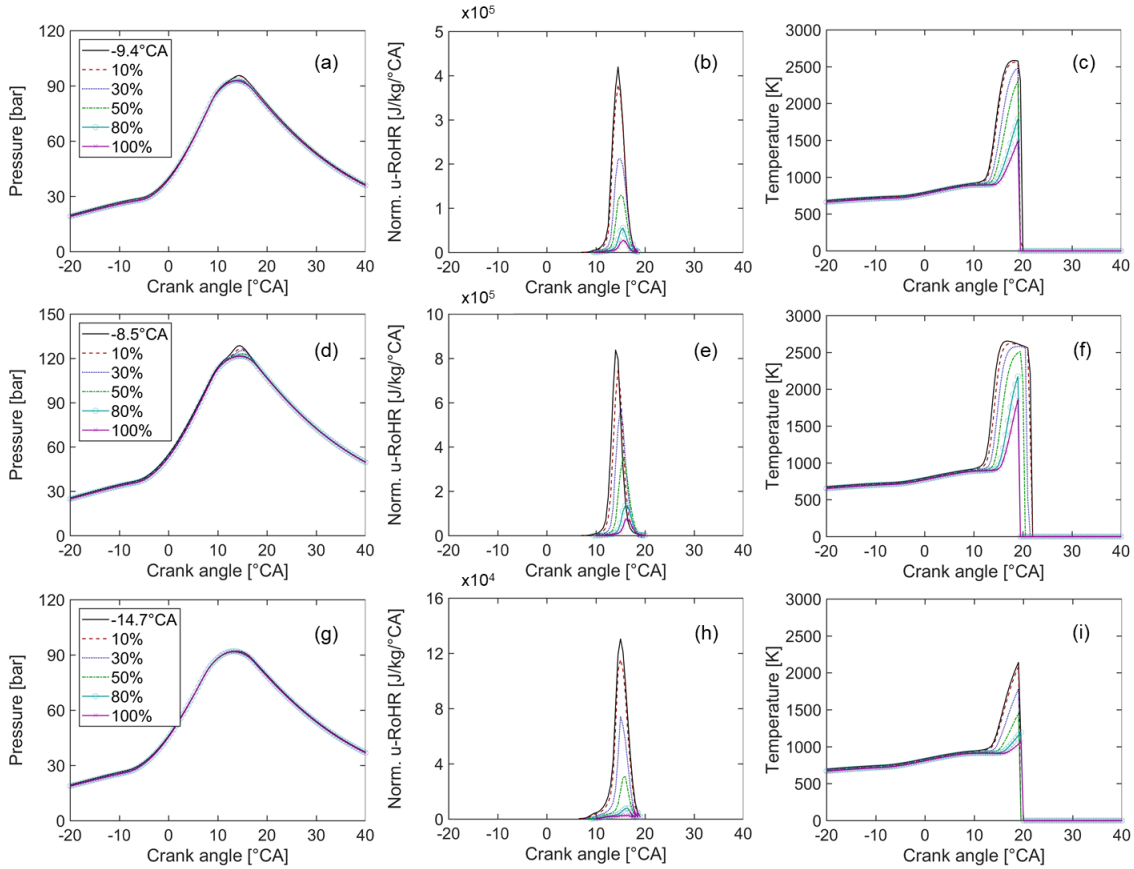


**Figure 14:** QD-SRM simulation results of in-cylinder pressure, normalized heat release rate in the end gas and temperature in the end gas for a Methanol fuel fraction sweep: (a) – (c) 1500 rpm 15 bar IMEP, (d) – (f) 2000 rpm 20 bar IMEP and (g) – (i) 2500 rpm 15 bar IMEP. Fired TDC is at 0 °CA.

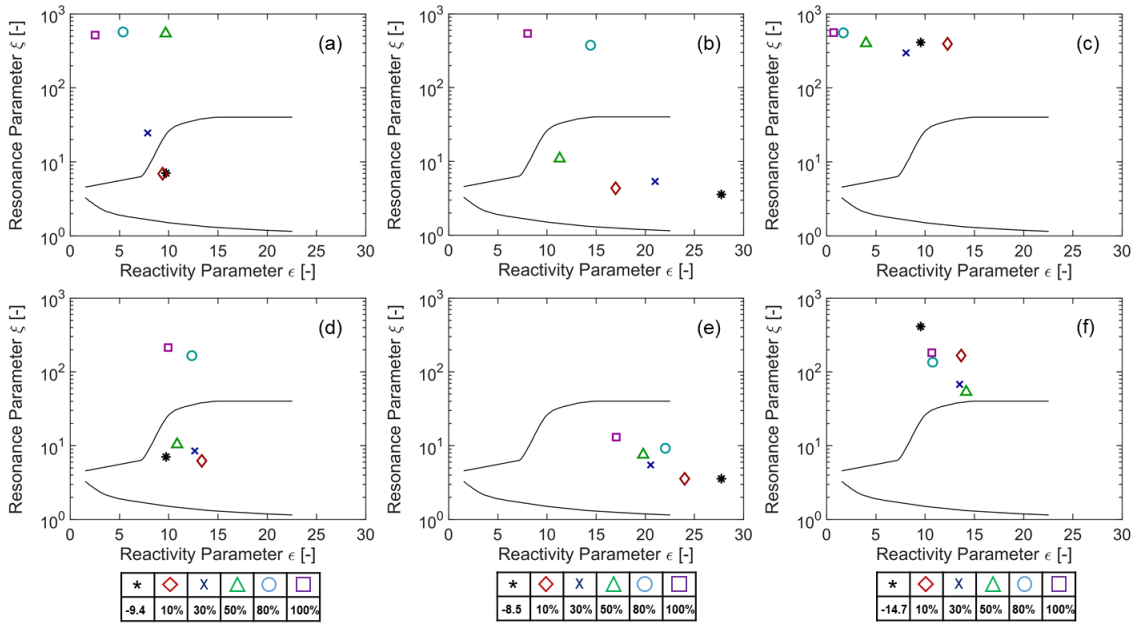


**Figure 15:** QD-SRM simulation results of the detonation diagram for a Methanol fuel fraction sweep: (a) 1500 rpm 15 bar IMEP with vaporization enthalpy, (b) 2000 rpm 20 bar IMEP with vaporization enthalpy, (c) 2500 rpm 15 bar IMEP with vaporization enthalpy, (d) 1500 rpm 15 bar IMEP without vaporization enthalpy, (e) 2000 rpm 20 bar IMEP without vaporization enthalpy and (f) 2500 rpm 15 bar IMEP without vaporization enthalpy.

### 5.4 Effect of Toluene Addition

The simulation results for in-cylinder pressure, normalized heat release rate and temperature in the end gas are depicted in **Figure 16 (a) to (i)**. The increase of Toluene fuel fraction in the fuel blend reduces the normalized heat release rate and temperature in the end gas. This is an effect of the larger ignition delay time of Toluene compared to RON95 E10 as shown in **Figure 2**.
The Detonation Diagram in **Figure 17** shows that even a small amount of Toluene in the gas mixture has a large effect on the auto-ignition in the end gas. At 1500 *rpm* 15 *bar* IMEP the addition of 0 *%* to 10 *%* Toluene fuel fraction to the fuel blend shifts the auto-ignition to subsonic conditions. At 2000 *rpm* 20 *bar* IMEP the addition of 10 *%* to 30 *%* Toluene fuel fraction to the fuel blend moves the auto-ignition out of the knocking combustion region. While the 2500 *rpm* 15 *bar* IMEP operating point is not knock limited at MBT operation, it also shows a reduced heat release rate in the end gas with increased amount of Toluene.
While Toluene is quite effective in reducing the auto-ignition in the end gas compared to Methanol, it has to be pointed out that higher amounts of aromatics in the fuel blend increase the formation of HC and soot emissions [57].

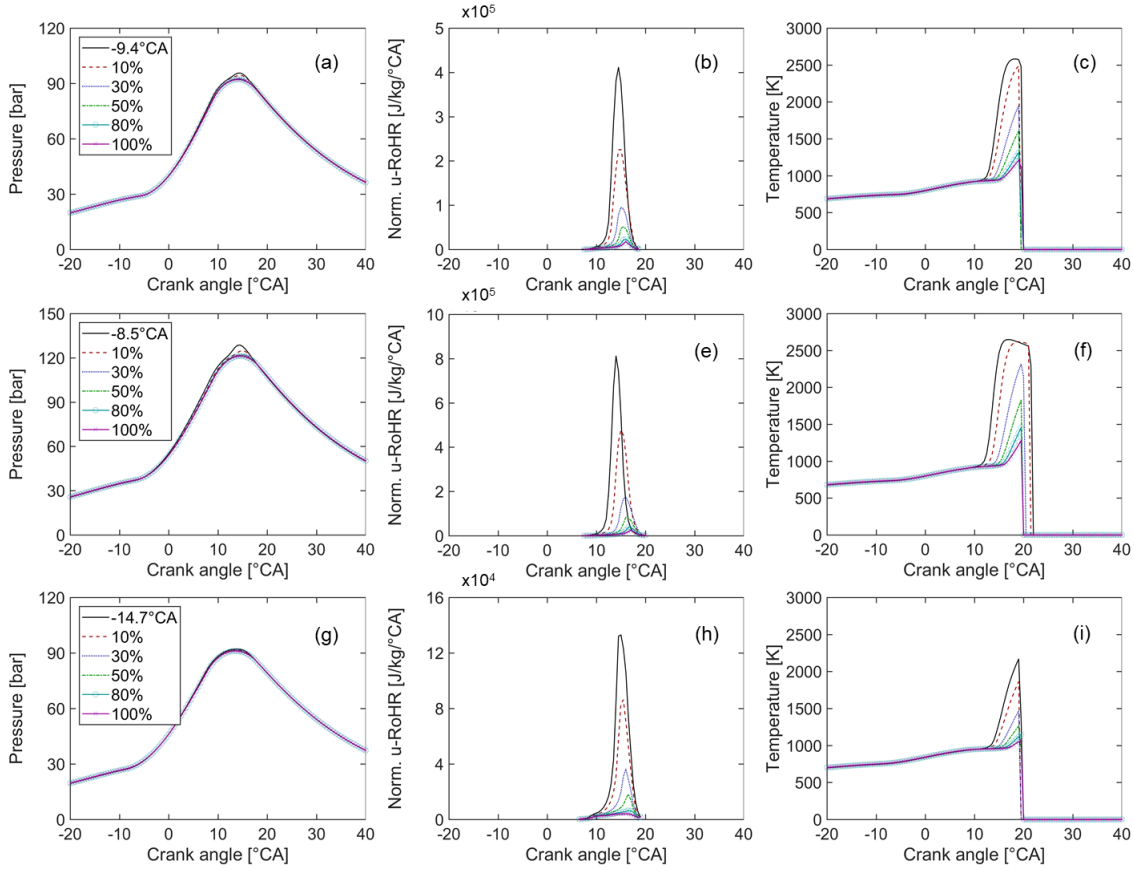


**Figure 16:** QD-SRM simulation results of in-cylinder pressure, normalized heat release rate in the end gas and temperature in the end gas for a Toluene fuel fraction sweep: (a) – (c) 1500 rpm 15 bar IMEP, (d) – (f) 2000 rpm 20 bar IMEP and (g) – (i) 2500 rpm 15 bar IMEP. Fired TDC is at 0 °CA.

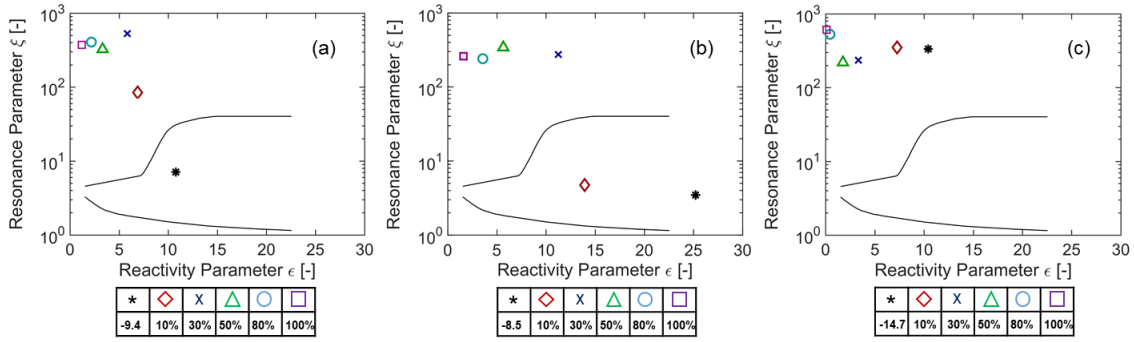


**Figure 17:** QD-SRM simulation results of the detonation diagram for a Toluene fuel fraction sweep: (a) 1500 rpm 15 bar IMEP with vaporization enthalpy, (b) 2000 rpm 20 bar IMEP with vaporization enthalpy and (c) 2500 rpm 15 bar IMEP with vaporization enthalpy.

### 5.5 Effect of Hydrogen Addition

The simulation results of Hydrogen addition to the fuel blend are shown in **Figure 18 (a) to (i)**. The charge pressure is increased for cases with higher Hydrogen fuel fraction in the fuel blend to keep the IMEP constant. The laminar flame speed is significantly increased with more Hydrogen fuel fraction in the fuel blend and the gradient of cylinder pressure during flame propagation becomes larger due to the higher laminar flame speeds. Further, the addition of Hydrogen to the fuel blend increases the reactivity of the gas mixture and the auto-ignition heat release rate is increased with increasing Hydrogen fuel fraction. Due to the late spark timing of the operating point at 2000 *rpm* 20 *bar* IMEP the normalized heat release rate is not increasing as much as for the other two operating points since the temperature is already decreased at that crank angle in the expansion stroke.

The detonation diagram in **Figure 19 (a) to (c)** highlights the increasing reactivity of the gas mixture due to higher Hydrogen fuel fraction. For the operating point at 1500 *rpm* 15 *bar* IMEP and 2500 *rpm* 15 *bar* IMEP the addition of 30 *%* to 50 *%* Hydrogen fuel fraction to the fuel blend leads to a developing detonation. At 2000 *rpm* 20 *bar* IMEP the addition of Hydrogen shows an increasing reactivity of the mixture but due to the lower temperature at which auto-ignition occurs, the reaction front velocity and pressure wave are not accelerated as much as for the other two operating points, wherefore the resonance parameter stays at a higher level. The reversed auto-ignition trend at 1500 *rpm* and 15 *bar* IMEP and 2500 *rpm* and 15 *bar* IMEP for 80 % and 100 % Hydrogen fuel fraction in the fuel blend, is because of decreasing local temperature and pressure at the advanced crank angles at which auto-ignition occurs.

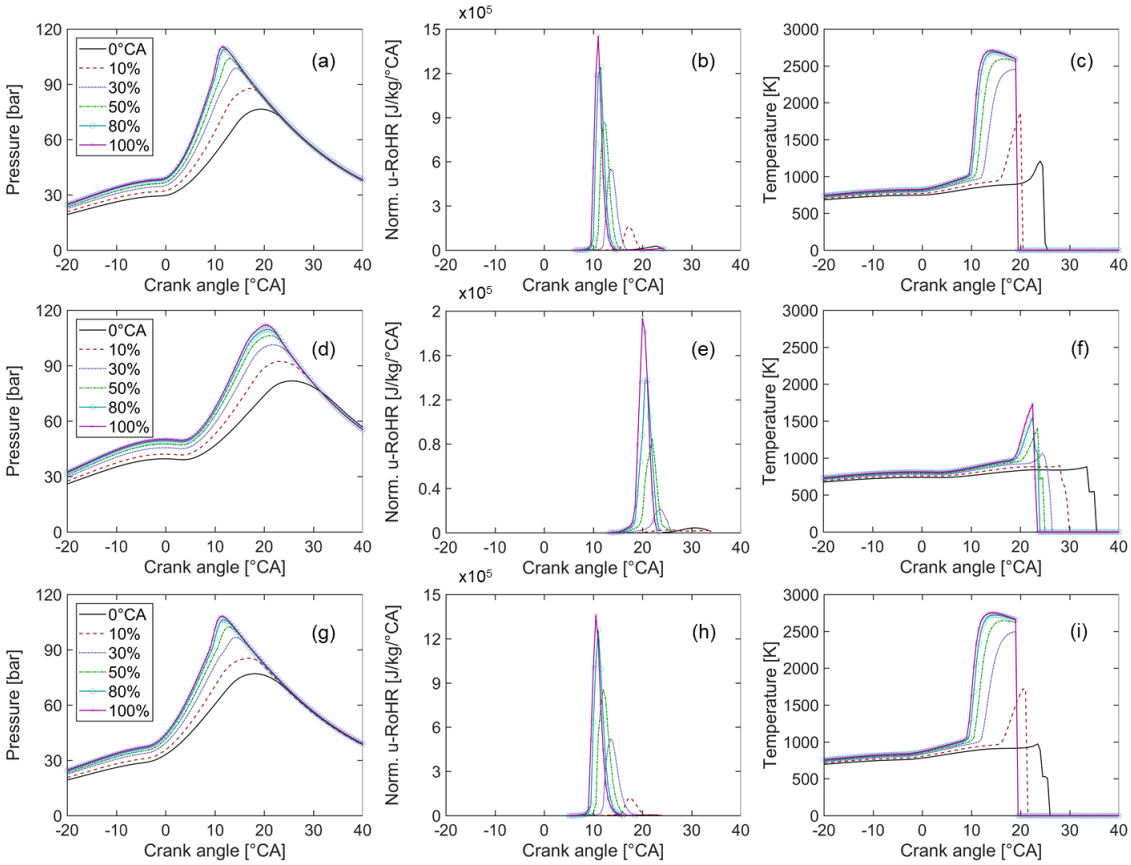


**Figure 18:** QD-SRM simulation results of in-cylinder pressure, normalized heat release rate in the end gas and temperature in the end gas for a Hydrogen fuel fraction sweep: (a) – (c) 1500 rpm 15 bar IMEP, (d) – (f) 2000 rpm 20 5bar IMEP and (g) – (i) 2500 rpm 15 bar IMEP. Fired TDC is at 0 °CA.

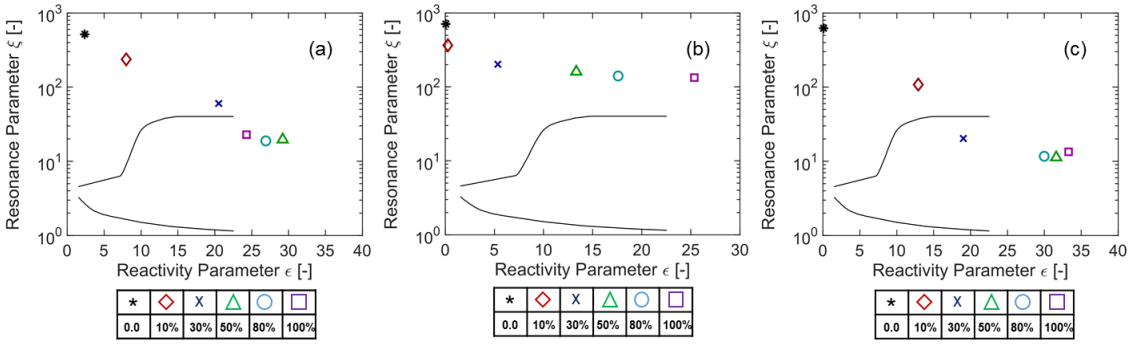


**Figure 19:** QD-SRM simulation results of the detonation diagram for a Hydrogen fuel fraction sweep: (a) 1500 rpm 15 bar IMEP, (b) 2000 rpm 20 bar IMEP and (c) 2500 rpm 15 bar IMEP.

## 6. Conclusions

This work outlines the assessment of different RON95 E10, Methanol, Toluene and Hydrogen blends regarding its effect on the auto-ignition modes in the end gas of a SI engine. It illustrates a novel simulation approach to jointly assess engine operating conditions and fuel blends and its effect on knocking combustion. The methodology is based on numerical investigations using the QD-SRM, dual-fuel tabulated chemistry look-up tables and the detonation diagram. The following conclusions are drawn based on the simulation results:

- The vaporization enthalpy of Methanol has a strong effect on the decreasing auto-ignition tendency of RON95 E10 and Methanol fuel blends. The engine can be operated at MBT at 1500 *rpm* and 15 *bar* IMEP, with 10 *%* to 30 *%* Methanol fuel fraction in the fuel blend and at 2000 *rpm* 20 *bar* IMEP, with 50 *%* to 80 *%* Methanol fuel fraction in the fuel blend.
- Toluene is highly effective in reducing the auto-ignition tendency for all operating conditions due to the longer ignition delay times. In contrast to Methanol the heat of vaporization is not the major factor, but the fuel chemistry, in particular the absence of a low temperature regime for Toluene. Compared to Methanol, only small additional amounts of Toluene in the fuel blend are needed to operate at MBT without knocking combustion. At 1500 *rpm* 15 *bar* IMEP up to 10 *%* additional Toluene fuel fraction are needed in the fuel blend and at 2000 *rpm* 20 *bar* IMEP 10 *%* to 30 *%* additional Toluene fuel fraction in the fuel blend are needed.
- The addition of Hydrogen decreases the burn duration, increases the PCP and increases the reactivity of the mixture in the end gas. The addition of 30 *%* Hydrogen fuel fraction in the fuel blend at 1500 *rpm* 15 *bar* IMEP corresponds to 6 °*CA* advancement of the spark timing. At 2500 *rpm* 15 *bar* IMEP the addition of 30 *%* Hydrogen fuel fraction in the fuel blend corresponds to 8 °*CA* to 10 °*CA* advancement of the spark timing.
- The QD-SRM simulation with tabulated chemistry and knock analysis takes 9 seconds for one engine cycle on 1 Intel Multi-Core i7-7820HQ CPU @ 2.90 GHz.

The future work consists of the following work steps:

- Extend the analysis for lean operation and increased compression ratios.
- Extend the analysis for different reaction mechanisms.
- Extend the analysis for other fuel blends.

## References

[1] J. Farrell, J. Holladay und R. Wagner, „Fuel Blendstocks with the Potential to Optimize Future Gasoline Engine Performance," NREL TP-5400-69009, 2018.

[2] U. Kramer, S. Stollenwerk, F. Ortloff, X. Sava, A. Janssen, S. Eppler, H. Schüle, A. Döhler, R. Otten, M. Lohrmann, L. Menger, S. Barth, W. Kübler und R. Thee, „Climate-neutral driving in 2050: Options for the complete defossilization of the transport sector," Forschungsvereinigung Verbrennungsmotoren, Frankfurt am Main, 2019.

[3] J. Vancoillie, J. Demuynck, L. Sileghem, M. Van De Ginste, S. Verhelst, L. Brabant und L. Van Hoorebeke, „The potential of methanol as a fuel for flex-fuel and dedicated spark-ignition engines," *Applied Energy, Vol. 102,* pp. 140-149, 2013.

[4] J. Vancoillie, J. Demuynck, L. Sileghem, M. Van De Ginste und S. Verhelst, „Comparison of the renewable transportation fuels, hydrogen and methanol formed from hydrogen, with gasoline - Engine efficiency study," *International Journal of Hydrogen Energy,* Bd. 37, pp. 9914-9924, 2012.

[5] K. Mueller, F. Rachow, V. Guenther und D. Schmeißer, „Methanation of Coke Oven Gas with Nickel-based catalysts," *International Journal of Environmental Science, Vol. 4,* pp. 73-79, 2019.

[6] F. Rachow, M. Hagendorf, K. Mueller und D. Schmeißer, „Synthesis of Methanol from CO2 for Power-to-Liquid applications," in *Verhandlungen der Deutschen Physikalischen Gesellschaft*, Bad Honnef, 2017.

[7] D. Gschwend, P. Soltic, A. Wokaun und F. Vogel, „Review and Performance Evaluation of Fifty Alternative Liquid Fuels for Spark-Ignition Engines," *Energy & Fuels, Vol. 33,* pp. 2186-2196, 2019.

[8] N. Yokoo, Y. Miyamoto, K. Nakata, K. Obata, G. Aoki und M. Watanabe, „Research of Fuel

Components to Enhance Engine Thermal Efficiency," Society of Automotive Engineers of Japan, Vol. 50, 2019.

[9] E. W. Lemmon, M. L. Huber und M. O. McLinden, „NIST Standard Reference Database 23," U.S. Secretary of Commerce, 2013.

[10] LOGE AB, „LOGEtable v2.0," 2020. [Online]. Available: https://logesoft.com. [Zugriff am 30 April 2020].

[11] LOGE AB, „LOGEfuel," 2020. [Online]. Available: https://logesoft.com. [Zugriff am 30 April 2020].

[12] K. P. Shrestha, L. Seidel, T. Zeuch und F. Mauss, „Detailed Kinetic Mechanism for the Oxidation of Ammonia Including the Formation and Reduction of Nitrogen Oxides," *Energy & Fuels, Vol. 32,* pp. 10202-10217, 2018.

[13] K. P. Shrestha, L. Seidel, T. Zeuch und F. Mauss, „Kinetic Modeling of NOx Formation and Consumption during Methanol and Ethanol Oxidation," *Combustion Science and Technology, Vol. 191,* pp. 1628-1660, 2019.

[14] K. P. Shrestha, N. Vin, O. Herbinet, L. Seidel, F. Battin-Leclerc, T. Zeuch und F. Mauss, „Insights into nitromethane combustion from detailed kinetic modeling – Pyrolysis experiments in jet-stirred and flow reactors," *Fuel, Vol. 261,* 2020.

[15] K. P. Shrestha, S. Eckart, A. M. Elbaz, B. R. Giri, C. Fritsche, L. Seidel, W. L. Roberts, H. Krause und F. Mauss, „A comprehensive kinetic model for Dimethyl ether and Dimethoxymethane oxidation and NOx interaction utilizing experimental laminar flame speed measurements at elevated pressure and temperature," *Combustion and Flame,* to be published.

[16] E. Ranzi, A. Frassoldati, R. Grana, A. Cuoci, T. Faravelli, A. P. Kelley und C. K. Law, „Hierarchical and comparative kinetic modeling of laminar flame speeds of hydrocarbon and oxygenated fuels," *Progress in Energy and Combustion Science,* Bd. 38, pp. 468-501, 2012.

[17] P. S. Veloo, Y. L. Wang, N. Egolfopoulos und C. K. Westbrook, „A comparative experimental and computational study of methanol, ethanol, and n-butanol flames," *Combustion and Flame,* Bd. 157, pp. 1989-2004, 2010.

[18] O. Mannaa, M. S. Mansour, W. L. Roberts und S. H. Chung, „Laminar burning velocities at elevated pressures for gasoline and gasoline surrogates associated with RON," *Combustion and Flame,* Bd. 162, pp. 2311-2321, 2015.

[19] C. Dong, Q. Zhou, Q. Zhao, Y. Zhang, T. Xu und S. Hui, „Experimental study on the laminar flame speed of hydrogen/carbon monoxide/air mixtures," *Fuel,* Bd. 88, pp. 1858-1863, 2009.

[20] K. Fieweger, R. Blumenthal und G. Adomeit, „Self-Ignition of SI Engine Model Fuels: A Shock Tube Investigation of High Pressure," *Combustion and Flame,* Bd. 109, pp. 599-619, 1997.

[21] U. Burke, W. K. Metcalfe, S. K. Burke, A. K. Heufer, P. Dagaut und H. J. Curran, „A detailed chemical kinetic modeling, ignition delay time and jet-stirred reactor study of methanol oxidation," *Combustion and Flame,* Bd. 165, pp. 125-136, 2016.

[22] J. C. G. Andrae, P. Björnbom, R. F. Cracknell und G. T. Kalghatgi, „Autoignition of toluene reference fuels at high pressures modeled with detailed chemical kinetics," *Combustion and Flame,* Bd. 149, pp. 2-24, 2007.

[23] A. Keromnes, W. K. Metcalfe, K. A. Heufer, N. Donohoe, A. K. Das, C.-J. Sung, J. Herzler, C. Naumann, P. Griebel, O. Mathieu, M. C. Krejci, E. L. Petersen, W. J. Pitz und H. J. Curran, „An experimental and detailed chemical kinetic modeling study of hydrogen and syngas mixture oxidation at elevated pressures," *Combustion and Flame,* Bd. 160, pp. 995-1011, 2013.

[24] F. Spausta, Eigenschaften und Untersuchungen der flüssigen Treibstoffe. Die gasförmigen Treibstoffe., Wien: Springer-Verlag, 1953.

[25] L. Seidel, Development and Reduction of a Multicomponent Reference Fuel for Gasoline, Cottbus: BTU Cottbus-Senftenberg, 2017.

[26] D. Bradley, C. Morley, X. J. Gu und D. R. Emerson, „Amplified Pressure Waves During Autoignition: Relevance to CAI Engines," *SAE Technical Paper, 2002-01 -2868,* 2002.

[27] X. J. Gu, D. R. Emerson und D. Bradley, „Modes of Reaction Front Propagation from Hot Spots," *Combustion and Flame,* Bd. 133, pp. 63-74, 2003.

[28] C. Netzer, Simulation and Assessment of Engine Knock Events, Cottbus: BTU Cottbus-Senftenberg, 2019.

[29] C. Netzer, L. Seidel, M. Pasternak, C. Klauer, C. Perlman, F. Ravet und F. Mauß, „Engine

Knock Prediction and Evaluation Based on Detonation Theory Using a Quasi-Dimensional Stochastic Reactor Model," *SAE Technical Paper, 2017-01-0538,* 2017.

[30] C. Netzer, L. Seidel, M. Pasternak, H. Lehtiniemi, C. Perlman, F. Ravet und F. Mauss, „Three-Dimensional Computational Fluid Dynamics Engine Knock Prediction and Evaluation based on Detailed Chemistry and Detonation Theory," *International Journal of Engine Research,* Bd. 19, Nr. 1, pp. 33-44, 2018.

[31] C. Netzer, L. Seidel, F. Ravet und F. Mauss, „Assessment of the Validity of RANS Knock Prediction using the Resonance Theory," *International Journal of Engine Research,* 2019.

[32] C. Netzer, L. Seidel, F. Ravet und F. Mauss, „Impact of the Surrogate Formulation on 3D CFD Engine Knock Prediction using Detailed Chemistry," *Fuel,* Bd. 254, 2019.

[33] M. Kraft, Stochastic Modeling of Turbulent Reacting Flow in Chemical Engineering, VDI Verlag, 1998.

[34] M. Tuner, Stochastic Reactor Models for Engine Simulations, Lund: Lund University, 2008.

[35] M. Pasternak, Simulation of the Diesel Engine Combustion Process Using the Stochastic Reactor Model, Berlin: LOGOS, 2016.

[36] R. L. Curl, „Dispersed Phase Mixing: I. Theory and Effects in Simple Reactors," *A.I.Ch.E. Journal,* Bd. 9, Nr. 2, pp. 175-181, 1962.

[37] M. Pasternak, F. Mauss, M. Sens, M. Riess, A. Benz und K. G. Stapf, „Gasoline Engine Simulations using Zero-Dimensional Spark Ignition Stochastic Reactor Model and Three-Dimensional Computational Fluid Dynamics Engine Model," *International Journal of Engine Research,* Bd. 17, Nr. 1, p. 76–85, 2016.

[38] M. Sens, A. Benz, M. Riess, F. G. Lage, X. S. Bjerkborn, F. Mauss und M. Pasternak, „Multiple Spark Plug Approach: Potential for Future Highly Diluted Spark Ignited Combustion," in *SIA Powertrain*, Versailles, 2015.

[39] A. Dulbecco, S. Richard, O. Laget und P. Aubret, „Development of a Quasi-Dimensional K-k Turbulence Model for Direct Injection Spark Ignition (DISI) Engines Based on the Formal Reduction of a 3D CFD Approach," *SAE Technical Paper, 2016-01-2229,* 2016.

[40] N. Peters, Turbulent Combustion, Cambridge: Cambridge University Press, 2000.

[41] S. Bjerkborn, K. Frojd und C. Perlman, „A Monte Carlo Based Turbulent Flame Propagation Model for Predictive SI In-Cylinder Engine Simulations Employing Detailed Chemistry for Accurate Knock Prediction," *SAE Technical Paper 2012-01-1680,* 2012.

[42] T. Franken, C. Klauer, M. Kienberg, A. Matrisciano und F. Mauß, „Prediction of Thermal Stratification in an Engine-like Geometry using a 0D Stochastic Reactor Model," *International Journal of Engine Research,* 2019.

[43] G. Woschni, „A Universally Applicable Equation for the Instantaneous Heat Transfer Coefficient in the Internal Combustion Engine," *SAE Technical Paper, 670931,* 1967.

[44] S. Jerzembeck, N. Peters, P. Pepiot-Desjardins und H. Pitsch, „Laminar Burning Velocities at High Pressure for Primary Reference Fuels and Fasoline: Experimental and Numerical Investigation," *Combustion and Flame,* Bd. 156, Nr. 2, pp. 292-301, 2009.

[45] H. Lehtiniemi, A. Borg und F. Mauß, „Combustion Modeling of Diesel Sprays," *SAE Technical Paper, 2016-01-0592,* 2016.

[46] H. Lehtiniemi, F. Mauß, M. Balthasar und I. Magnusson, „Modeling Diesel Spray Ignition using Detailed Chemistry with a Progress Variable Approach," *Combustion Science and Technology,* Bd. 178, pp. 1977-1997, 2006.

[47] A. Matrisciano, T. Franken, C. Perlman, A. Borg, H. Lehtiniemi und F. Mauss, „Development of a Computationally Effcient Progress Variable Approach for a Direct Injection Stochastic Reactor Model," *SAE Technical Paper, 2017-01-0512,* 2017.

[48] A. Matrisciano, A. Borg, C. Perlman und H. Lehtiniemi, „Soot Source Term Tabulation Strategy for Diesel Engine Simulations with SRM," *SAE Technical Paper, 2015-24-2400,* 2015.

[49] Peters, N., Kerschgens, B. and Paczko, G., „Super-Knock Prediction Using a Refined Theory of Turbulence," *SAE International Journal of Engines, ,* Bd. 6, Nr. 2, pp. 953-967, 2013.

[50] L. Bates, D. Bradley, G. Paczko and N. Peters, "Engine hotpots: Modes of Auto-Ignition and Reaction Propagation," *Combustion and Flame,* vol. 166, pp. 80-85, 2016.

[51] Y. B. Zeldovich, „Regime Classification of an Exothermic Reaction with Nonuniform Initial

Conditions," *Combustion and Flame,* Bd. 39, pp. 211-214, 1980.

[52] D. Bradley, „Autoignitions and Detonations in Engines and Ducts," *Philosophical Transactions of the Royal Society,* Bd. 370, pp. 689-714, 2012.

[53] G. T. Kalghatgi und D. Bradley, „Pre-ignition and 'Super-Knock' in Turbocharged Spark-Ignition Engines," *SAE International Journal of Engines,* Bd. 13, Nr. 4, pp. 399-414, 2015.

[54] ESTECO, „modeFRONTIER User Guide 2018R1," 2018. [Online]. Available: https://www.esteco.com/modefrontier.

[55] T. Franken, F. Mauss, L. Seidel, M. S. Gern, M. Kauf, A. Matrisciano und A. C. Kulzer, „Gasoline engine performance simulation of water injection and low-pressure exhaust gas recirculation using tabulated chemistry," *International Journal of Engine Research,* 2020.

[56] T. Franken, L. Seidel, A. Matrisciano, F. Mauss, A. C. Kulzer und F. Schuerg, „Analysis of the Water Addition Efficiency on Knock Suppression for Different Octane Ratings," *SAE Technical Paper, 2020-01-0551,* 2020.

[57] G. Karavalakis, D. Short, D. Vu, R. Russell, M. Hajbabaei, A. Asa-Awuku und T. D. Durbin, „Evaluating the Effects of Aromatics Content in Gasoline on Gaseous and Particulate Matter Emissions from SI-PFI and SIDI Vehicles," *Environmental Schience & Technology,* Bd. 49, pp. 7021-7031, 2015.